Inorganic Chemistry
Article

Inorg. Chem. **2009**, *48*, 11559–11565 **11559**
DOI: 10.1021/ic901829v

Hydrothermal Synthesis and Luminescent Properties of Novel Ordered Sphere $CePO_4$ Hierarchical Architectures

Mei Yang,[†,‡] Hongpeng You,[*,†] Yuhua Zheng,[†,‡] Kai Liu,[†,‡] Guang Jia,[†,‡] Yanhua Song,[†,‡] Yeju Huang,[†,‡] Lihui Zhang,[†,‡] and Hongjie Zhang[*,†]

[†]*State Key Laboratory of Rare Earth Resource Utilization, Changchun Institute of Applied Chemistry, Chinese Academy of Sciences 130022, and* [‡]*Graduate University of the Chinese Academy of Sciences, Beijing 100049, P. R. China*

Received June 21, 2009

The ordered-sphere $CePO_4$ hierarchical architectures have been successfully synthesized by a simple hydrothermal method through the controlled growth of the $CePO_4$ nanorods and self-assemble hierarchical structure under various reaction conditions. The evolution of the morphology of the samples has been investigated in detail. It was found that the coexistence of citric acid and cetaltrimethylammonium bromide in the reaction system plays an important role in the formation of the spherical $CePO_4$ hierarchical architectures. A possible mechanism of the formation and growth of the hierarchical structure was suggested according to the experimental results and analysis. The effects of the reaction time as well as the variation of the morphologies on the luminescent properties of the products were also studied.

1. Introduction

In recent years, large-scale hierarchical self-assembly structures from basic building blocks with specific morphology and novel properties have attracted considerable interest for their potential technology applications because their unique properties are determined by their morphology, size, and dimensions. Many efforts have thus been made recently to develop new methods for the fabrication of hierarchical ordered structures in material chemistry.[1,2] Although some progress has been made in the self-assembly of highly organized building blocks of metals,[3] semiconductors,[4,5] copolymers,[6] organic−inorganic hybrid materials,[7] and biomaterials[8] based on different driving mechanisms, effective large-scale hierarchical self-assembly of some functional materials is still a challenge to material scientists.

Recently, much attention has been focused on the synthesis and photoluminescence properties of lanthanide orthophosphates ($LnPO_4$) and lanthanide (III)-doped lanthanide orthophosphates ($LnPO_4$:Ln^{3+}) because of their potential applications in color displays,[9,10] field-effect transistors,[11,12] optoelectronics,[13] medical and biological labels,[14] solar cells,[15,16] and light sources.[17,18] To date, various lanthanide orthophosphate nanomaterials, such as zero-dimensional nanoparticles,[20,21] one-dimensional (1D) structures,[22,23] and core/shell structures,[24] have been successfully synthesized.

*To whom correspondence should be addressed. Tel.: 86431- 85692798. Fax: 86431-85698041. E-mail: hpyou@ciac.jl.cn (H.Y.), hongjie@ciac.jl.cn (H.Z.).

(1) Zhu, L. P.; Xiao, H. M.; Zhang, W. D.; Yang, Y.; Fu, S. Y. *Cryst. Growth Des.* **2008**, *8*, 1113.
(2) Jung, S. H.; Oh, E.; Lee, K. H; Yang, Y.; Park, C. G.; Park, W. J.; Jeong, S. H. *Cryst. Growth Des.* **2008**, *8*, 1265.
(3) Kaltenpoth, G.; Himmelhaus, M.; Slansky, L.; Caruso, F.; Grunze, M. *Adv. Mater.* **2003**, *15*, 1113.
(4) Yada, M.; Taniguchi, C.; Torikai, T.; Watari, T.; Furuta, S.; Katsuki, H. *Adv. Mater.* **2004**, *16*, 1448.
(5) Fan, H. Y.; Yang, K.; Boye, D. M.; Sigmon, T.; Malloy, K. J.; Xu, H.; López, G. P.; Brinker, C. J. *Science* **2004**, *304*, 567.
(6) (a) Jenekhe, S. A.; Chen, X. L. *Science* **1998**, *279*, 1903. (b) Ikkala, O.; Brinke, G. T. *Science* **2002**, *295*, 2407.
(7) Du, J.; Chen, Y. *Angew. Chem., Int. Ed.* **2004**, *43*, 5084.
(8) Shenton, W.; Pum, D.; Sleytr, U. B.; Mann, S. *Nature* **1997**, *389*, 585.
(9) Lee, M. H.; Oh, S. G.; Yi, S. C.; Seo, D. S.; Hong, J. P.; Kim, C.; Yoo, Y. K.; Yoo, J. S. *J. Electrochem. Soc.* **2000**, *147*, 3139.
(10) Wang, Q. H.; Setlur, A. A.; Lauerhaas, J. M.; Dai, J. Y.; Seelig, W.; Chang, R. P. H. *Appl. Phys. Lett.* **1998**, *72*, 2912.
(11) Sun, B.; Sirringhaus, H. *Nano Lett.* **2005**, *5*, 2408.
(12) Talapin, D. V.; Murray, C. B. *Science* **2005**, *310*, 86.
(13) Huang, Y.; Lieber, C. M. *Pure Appl. Chem.* **2004**, *76*, 2051.
(14) Wang, L.; Yang, C. Y.; Tan, W. H. *Nano Lett.* **2005**, *5*, 37.
(15) Law, M.; Greene, L. E.; Johnson, J. C.; Saykally, R.; Yang, P. D. *Nat. Mater.* **2005**, *4*, 455.
(16) Shalav, A.; Richards, B. S.; Trupke, T.; Kramer, K. W.; Gudel, H. U. *Appl. Phys. Lett.* **2005**, *86*, 13505.
(17) Choi, H. J.; Johnson, J. C.; He, R. R.; Lee, S. K.; Kim, F.; Pauzauskie, P.; Goldberger, J.; Saykally, R. J.; Yang, P. D. *J. Phys. Chem. B* **2003**, *107*, 8721.
(18) Johnson, J. C.; Choi, H. J.; Knutsen, K. P.; Schaller, R. D.; Yang, P. D.; Saykally, R. J. *Nat. Mater.* **2002**, *1*, 106.
(20) Schuetz, P.; Caruso, F. *Chem. Mater.* **2002**, *14*, 4509.
(21) Xing, Y.; Li, M.; Davis, S. A.; Mann, S. *J. Phys. Chem. B.* **2006**, *110*, 3.
(22) Meyssamy, H.; Riwotzki, K.; Kornowski, A.; Naused, S.; Haase, M. *Adv. Mater.* **1999**, *11*, 840.
(23) Buissette, V.; Moreau, M.; Gacoin, T.; Boilo, J. P. *Adv. Funct. Mater.* **2006**, *16*, 351.
(24) Lehmann, O.; Kömpe, K.; Haase, M. *J. Am. Chem. Soc.* **2004**, *126*, 14935.

Published on Web 11/13/2009

However, reports on the hierarchical self-assembly of multidimensional $LnPO_4$ are still few,[25] although many different kinds of low-dimensional lanthanide phosphate nanomaterials have been reported.

In this paper, we provide a new example for the controlled growth of ordered-sphere flower-like $CePO_4$ hierarchical architectures synthesized using a hydrothermal method with the addition of cetaltrimethylammonium bromide (CTAB) as a surfactant and citric acid as a chelating reagent. The influence of the reaction conditions on the morphology and the properties of the products were investigated, and a possible formation mechanism of the architectures was proposed. The obtained architectures may have potential applications in the fields of optoelectronic devices. Moreover, our method may provide a new possibility to synthesize other materials with desired architectures.

2. Experimental Section

2.1. Synthesis of $CePO_4$. Citric acid monohydrate ($C_6H_8O_7 \cdot H_2O$), CTAB, and $(NH_4)_2HPO_4 \cdot 12H_2O$ were purchased from Beijing Chemical Corporation. $Ce(NO_3)_3 \cdot 6H_2O$ was purchased from Wuxi Yiteng Rare-Earth Limited Corporation. All reagents were analytical grade and were used as-received without further purification.

In a typical synthesis, 2 mmol of $Ce(NO_3)_3 \cdot 6H_2O$ and 3 mmol of $C_6H_8O_7 \cdot H_2O$ were first dissolved in deionized water. An ethanol−water solution containing 3 mmol of CTAB and 3 mmol of $(NH_4)_2HPO_4 \cdot 12H_2O$ was then added into the obtained solution. A transparent solution was obtained when 3 mL of HNO_3 was added into the solution drop by drop. After this process, the resulting solution was transferred into a Teflon-lined autoclave and sealed tightly. Then, the autoclave was maintained at 90 °C for 1−10 h. After cooling to room temperature naturally, the precipitate was collected and washed with deionized water and ethanol several times. The final products were dried at 60 °C for 12 h in the air.

The proportions of the ethanol to water (v/v) for the obtained samples were 1/35, 6/30, 11/25, 16/20, and 21/15, and the corresponding products were labeled as **S1**, **S2**, **S3**, **S4**, and **S5**, respectively.

2.2. Characterization. The X-ray diffraction (XRD) pattern was measured with a Rigaku-D X-Ray Powder Diffractometer with Cu Ka radiation (λ = 1.5418 Å). Fourier-transform infrared spectroscopy (FT-IR) spectra were measured with a BRUKER Vertex 70 FTIR using the KBr pellet technique. The morphology of the samples was inspected using a field emission scanning electron microscope (HITACHI S-4800). Transmission electron microscopy (TEM) and high-resolution transmission electron microscopy (HRTEM) images and selected area electron diffraction (SAED) pattern were obtained on a JEOL-2100 microscope with an accelerating voltage of 200 kV. Excitation and emission spectra were recorded with a Hitachi F-4500 fluorescence spectrophotometer equipped with a 150 W xenon lamp as the excitation source. All of the measurements were performed at room temperature.

3. Results and Discussion

Figure 1 shows the XRD patterns of the five samples obtained at 90 °C for 10 h. It can be found that the peak positions of the XRD patterns agree well with those of the hexagonal phase $CePO_4$ in JCPDS file 34-1380, except that of **S1**, which has weak peaks indicated with "∗" (the weak peaks can be assigned to the monazite phase of $CePO_4$ in JCPDS file 32-0199). No additional peaks of other phases had been found in the other four samples, indicating that the proportion of ethanol to water has little effect on the phase formation of the products.

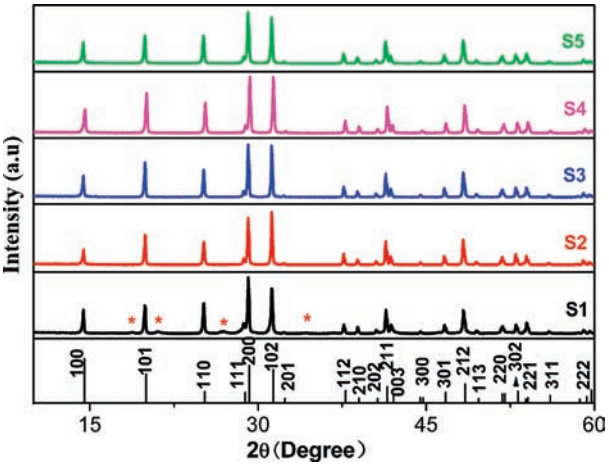

Figure 1. XRD patterns of **S1**−**S5** obtained at 90 °C for 10 h with different proportions of ethanol to water.

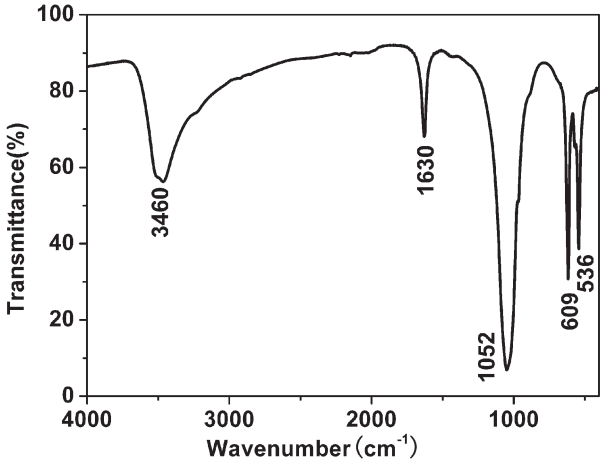

Figure 2. FT-IR spectrum of **S3** prepared at 90 °C for 10 h.

Figure 2 presents the typical FT-IR spectrum of **S3**. The bands centered at 1630 and 3460 cm^{-1} can be due to the water adsorbed on surface of the samples. The other bands are assigned to the phosphate groups. The band centered at 1052 cm^{-1} is ascribed to the asymmetry stretching vibration of the PO_4^{3-} groups, and the bands centered at 609 cm^{-1} and 536 cm^{-1} are attributed to the O−P−O bending vibrations.[26] The absorptions of N−H, C═O, and COO− are not observed in the FT-IR spectrum, indicating that the reagents of citric acid and CTAB remaining on the surface of the final products are so little that they cannot be detected.

Figure 3 shows the SEM images of the products obtained with different proportions of ethanol to water. When the proportion is 1/35, the aggregation type of the products is irregular, and most of them consisted of nanorods with diameters of 0.1−0.15 μm. In addition, there are still some regular hexagonal prisms with diameters of 0.8−1.6 μm in the product (Figure 3a). When the proportion is increased to

(25) Guan, M. Y.; Sun, J. H.; Han, M.; Xu, Z.; Tao, F. F.; Yin, G.; Wei, X. W.; Zhu, J. M.; Jiang, X. Q. *Nanotechnology* **2007**, *18*, 415602.

(26) Li, L.; Jiang, W. G.; Pan, H. H.; Xu, X. R.; Tang, Y. X.; Ming, J. Z.; Xu, Z. D.; Tang, R. K. *J. Phys. Chem. C* **2007**, *111*, 4111.

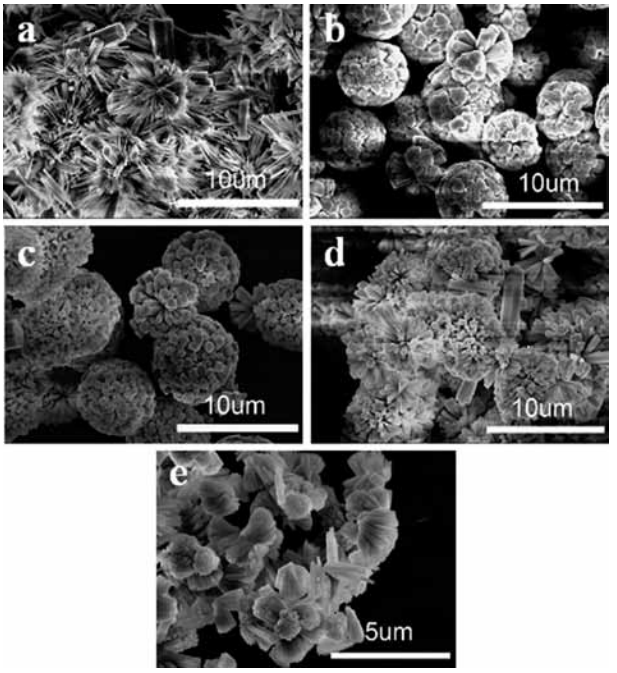

Figure 3. SEM images of **S1**−**S5** (a−e) obtained at 90 °C for 10 h with different proportions of ethanol to water. **S1**, 1/35; **S2**, 6/30; **S3**, 11/25; **S4**, 16/20; and **S5**, 21/15.

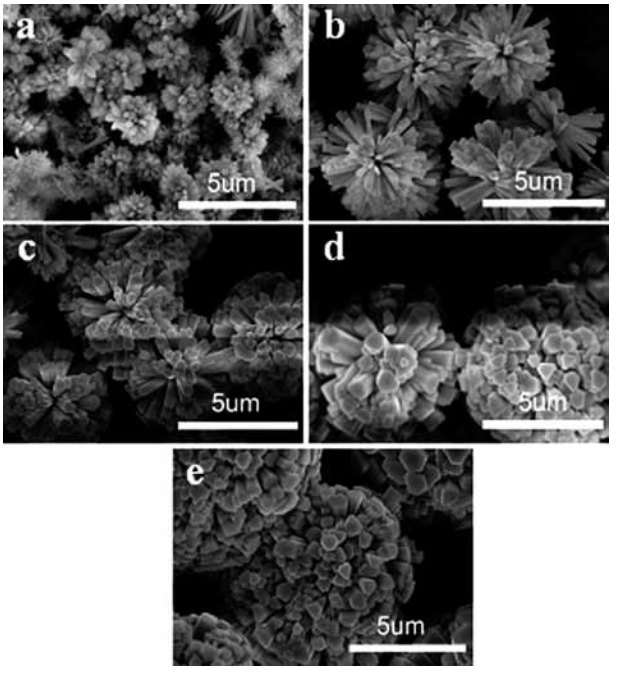

Figure 4. SEM images of the products obtained with different reaction times, with other reaction conditions similar to those for **S3**: a, 1 h; b, 1.5 h; c, 2.5 h; d, 5 h; e, 10 h.

6/30, the products display spherical flower-like hierarchical architectures with diameters of 5−6 μm (Figure 3b). The diameters of the prisms and architectures decrease gradually with the increase of the proportion of ethanol to water (Figure 3c,d). When the proportion is 21/15, the aggregation type of the product changes again: the nanoprisms self-assemble into a fanlike structure, and every fan is composed of numerous nanoprisms with a diameter of about 0.1 μm (Figure 3e). These results reveal that the proportion of ethanol to water has an important effect on the shape of the products.

In order to investigate the possible growth mechanism, the influences of reaction time and other reaction conditions were further investigated.

Figure 4 shows the SEM images of the products obtained with different reaction times. When the reaction time was 1 h, one can notice that the product is mainly flower-like microclusters composed of nanorods (Figure 4a). As the reaction time was increased, the small flower-like microclusters developed into larger spherical flower-like hierarchical architectures comprised of hexagonal prisms (Figure 4b). The diameters and lengths of the hexagonal prisms increased gradually with the reaction time. At the same time, some new small prisms in spherical flower-like architectures were formed. As a result, the comparative loose space among the prisms of the architectures became tight (Figure 4c−e). These results reveal that the formation of the spherical flower-like hierarchical architectures needs a certain time.

The product obtained at 90 °C for 1.5 h is further characterized by TEM, HRTEM, and SAED. Figure 5a displays the TEM image of the product, which is of perfect spherical assembly, confirming the above SEM observation. Figure 5c shows a typical HRTEM image of the selected prism (Figure 5b); the clear lattice fringes with a *d*-spacing of 0.61 nm belong to the lattice fringe of the (100) plane. Figure 5d shows the SAED pattern taken from the selected

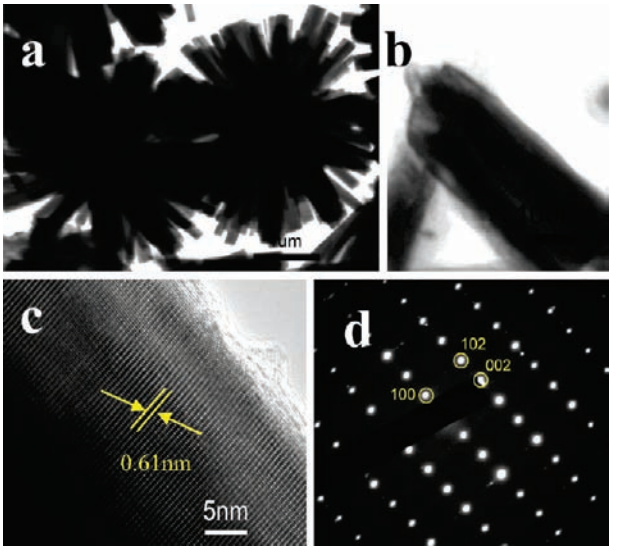

Figure 5. TEM and HRTEM images and SAED pattern of the product obtained at 90 °C for 1.5 h, with other reaction conditions similar to those for **S3**: a, low-magnification TEM image of the product; b, TEM image of an individual prism broken down from the hierarchical architecture; c, HRTEM image of the selected prism; d, SAED pattern taken from the selected prism.

prism. The indexes of the crystal faces are calculated, and the results shown in the image (Figure 5d) are consistent with the corresponding XRD pattern. Both the HRTEM image and the SAED pattern clearly demonstrate the single-crystalline nature of the prism.

The amount of HNO_3 added into the reaction solution also has an important effect on the morphologies of the products. Figure 6 displays the SEM images of the products obtained with different amounts of HNO_3 and other reaction conditions similar to those of **S3**. It can be noticed that spherical flower-like hierarchical architectures remain with an increase

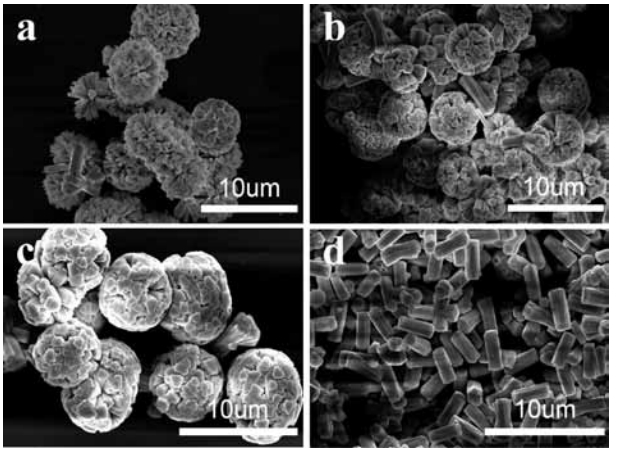

Figure 6. SEM images of the products obtained with different contents of HNO_3 and other reaction conditions similar to those for **S3**: a, 3.2 mL; b, 3.4 mL; c, 3.6 mL; d, 3.8 mL.

in the amount of HNO_3 lower than 3.6 mL, though the composed prisms grew larger gradually (Figure 6a−c). When the amount of HNO_3 increased to 3.8 mL, the prisms did not assemble together and form spherical flower-like hierarchical architectures; all of them remain single (Figure 6d). These results exhibit that the acidity of the solution also has an effect on the shape of the products.

During the experiment, it is worth noting that the amount of citric acid plays an important role in controlling the morphologies of the product. Figure 7 shows the SEM images of the products obtained with different amounts of citric acid and other reaction conditions similar to those of **S3**. Without the addition of citric acid into the reaction system, only nanorods were observed in the product (Figure7a). When the content of citric acid is 1.5 mmol, dandelion-like architectures with diameters of 4−6 μm were obtained. Every "dandelion" is comprised of numerous nanorods originating from the center (Figure 7b). As the content of citric acid was increased to 3 mmol, spherical flower-like hierarchical architectures were formed through the self-assembly of nanorods (Figure 7c). While the content of citric acid was further increased to 4.5 mmol, their diameters became larger and their shapes became elliptic (Figure 7d). These results indicate that appropriate content of citric acid is important for the formation of the flower-like $CePO_4$ hierarchical architectures.

Figure 8 shows the SEM images of the products obtained with different amounts of the CTAB and other reaction conditions similar to those for **S3**. It can be found that the architectures obtained without the addition of CTAB into the reaction system consist of a hexagonal prism in the middle and many small prisms tightly growing on its side without any space between them, but the shape of the surrounding prisms is not complete (Figure 8a, their lower and higher magnifications are shown in SP). When CTAB was added into the reaction system, the shape of the product changed dramatically, and spherical flower-like hierarchical architectures composed of prisms were formed. It is noted that the main shape of the product changes little with the increase of the content of CTAB (Figure 8b−d). Therefore, the existence of CTAB also plays an important role in the formation of the spherical flower-like hierarchical architectures.

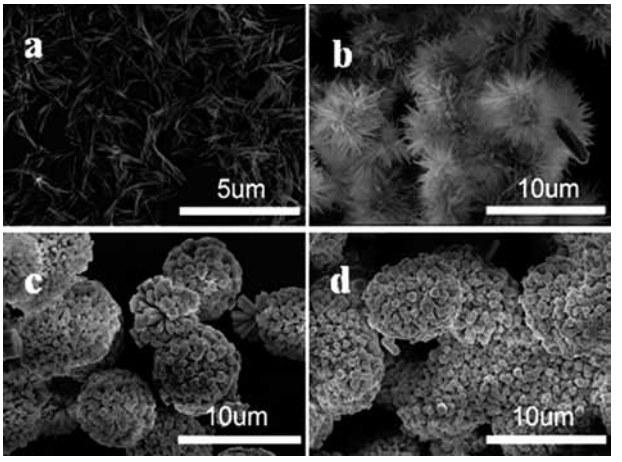

Figure 7. SEM images of the products obtained with different contents of citric acid and other reaction conditions similar to those for **S3**: a, 0 mmol citric acid; b, 1.5 mmol citric acid; c, 3 mmol citric acid; d, 4.5 mmol citric acid.

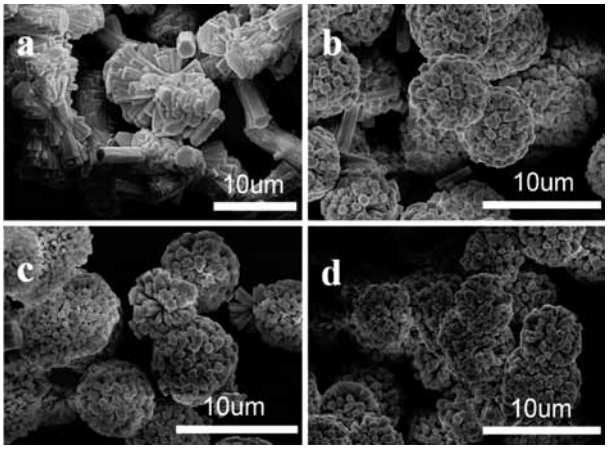

Figure 8. SEM images of the products obtained with different contents of CTAB and other reaction conditions similar to those for **S3**: a, 0 mmol CTAB; b, 1.5 mmol CTAB; c, 3 mmol CTAB; d, 4.5 mmol CTAB.

On the basis of the experimental results and analysis, it is reasonable to assume that the products may grow following the crystal splitting theory that was proposed by Tang and Alivisatos for the formation of the sheaf-like Bi_2S_3 hierarchical structure.[27] At the beginning of the reaction, $CePO_4$ nuclei were produced, which grew the building blocks for the hierarchical structure. In the following growth process, the nuclei grew into nanorods under the effects of the crystal structure and external powers. At the same time, branches were developed on the surroundings of the nanorods stems, leading to the splitting. This progress was a fast growth process. The growth rate of $CePO_4$ nuclei and the surfactant adsorbed on the crystal facet should play key roles in the formation of the final hierarchical architectures. As the reaction time increased, splitting growth continued, and the comparative loose space among the prisms of the architectures became tight gradually. The possible growth process of the product is shown in Figure 9.

The formation of one-dimensional hexagonal prisms should be the main result of the inner cell structure of hexagonal $CePO_4$. Figure 10 shows the simulated crystal

(27) Tang, J.; Alivisatos, A. P. *Nano Lett.* **2006**, *6*, 2701.

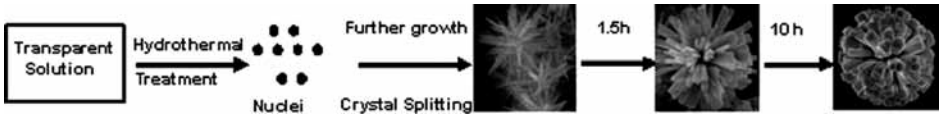

Figure 9. Possible growth process of the $CePO_4$ sphere flower-like hierarchical architecture.

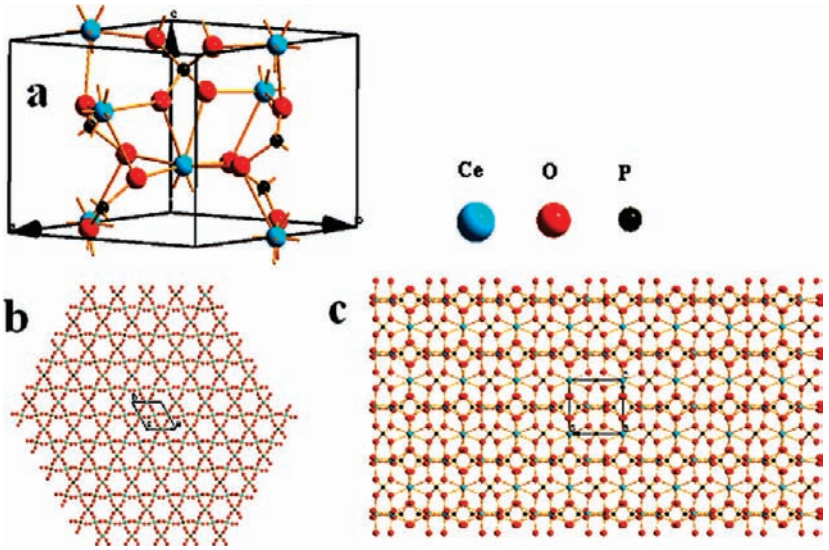

Figure 10. Simulated crystal structures of $CePO_4$: a, crystal structure; b, packing view along the *c* axis; c, packing view along the *a* axis.

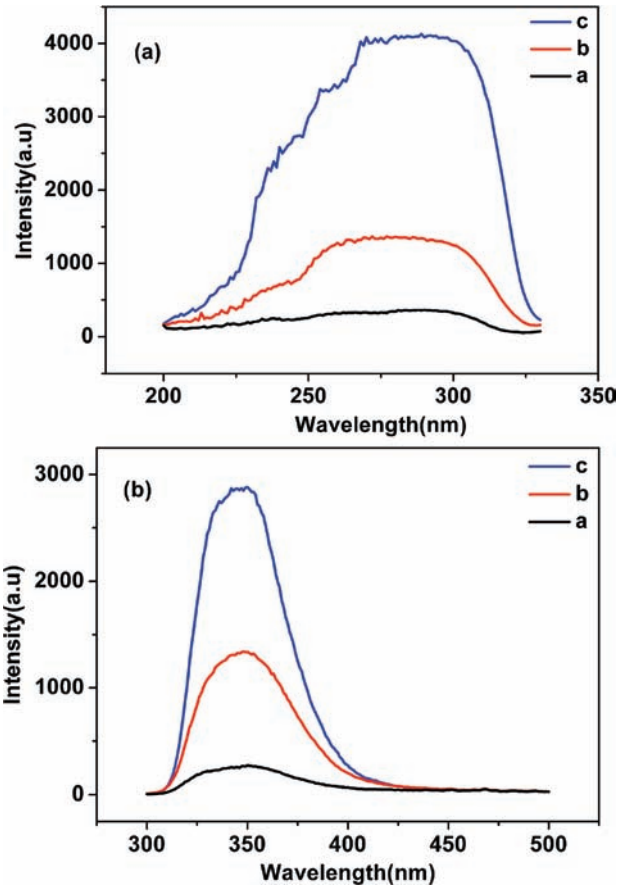

Figure 11. Excitation (a) and emission (b) spectra of the products obtained at different reaction times: a, 1 h; b, 1.5 h; c, 10 h (the three samples are measured by using the same experimental conditions).

structures of $CePO_4$. The overall structure of hexagonal $CePO_4$ can be described as columns built up of alternate cerium and phosphate ions, extending along the *c* axis, each column linked to four neighboring columns (Figure 10b). The packing structure of hexagonal $CePO_4$ viewed along the *a* axis can be described as infinite linear chains, parallel to the *c* axis (Figure 10c).[28] This 1D characteristic of the infinite linear chains of hexagonal-structured $CePO_4$ should play crucial roles in determining the one-dimensional hexagonal prisms.[29]

In addition, it is well-known that CTAB is a soft template which facilitates the growth of the 1D structure, and many researchers have used it to control the growth of the 1D structures.[30−32] CTAB can ionize completely in water. The resulting cation is a positively charged tetrahedron with a long hydrophobic tail, while PO_4^{3-} also has a tetrahedral geometry but is negatively charged. Therefore, ion pairs between CTA^+ and PO_4^{3-} could form due to electrostatic interaction. When an amount of CTAB is added to the reaction solution, the resulting CTA^+ ions adsorb on the surface of the nuclei and serve as a growth controller and an agglomeration inhibitor, which further inhibit the increase of the diameter of the prisms as well as the aggregation of the other nuclei on the formed crystals.[32]

(28) Mooney, R. C. L. *Acta Crystallogr.* **1950**, *3*, 337.
(29) Fang, Y. P.; Xu, A. W.; Song, R. Q.; Zhang, H. X.; You, L. P.; Jimmy, C. Y.; Liu, H. Q. *J. Am. Chem. Soc.* **2003**, *125*, 16025.
(30) Yan, R. X.; Sun, X. M.; Wang, X.; Peng, Q.; Li, Y. D. *Chem.—Eur. J.* **2005**, *11*, 2183–2195.
(31) Li, Y.; Li, Y. D.; Deng, Z. X.; Zhuang, J.; Sun, X. M. *Int. J. Inorg. Mater.* *3* **2001**, 633–637.
(32) Sun, X. M.; Chen, X.; Deng, Z. X.; Li, Y. D. *Mater. Chem. Phys.* **2002**, *78*, 99.

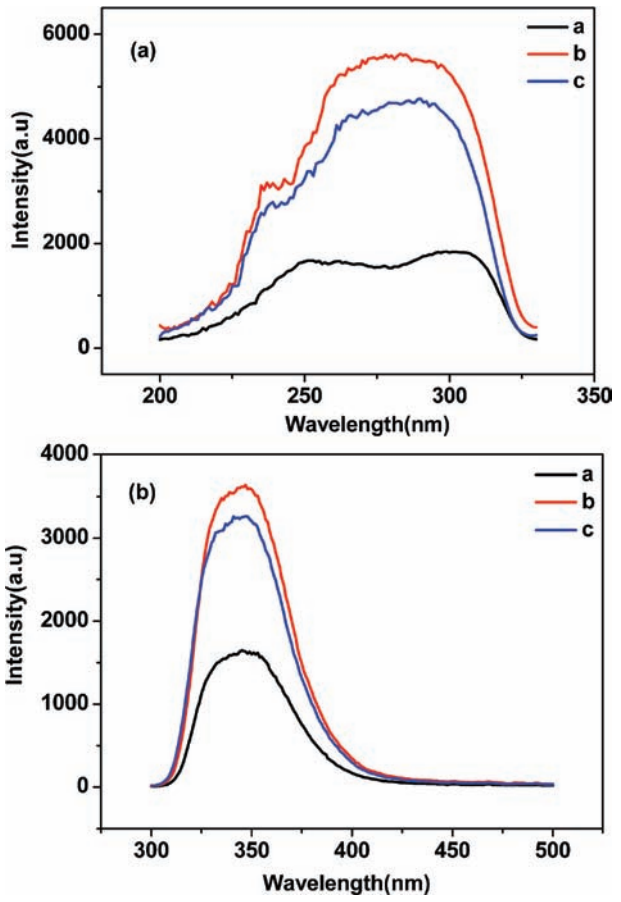

Figure 12. Excitation (a) and emission (b) spectra of the products with different morphologies: a, flower-like hierarchical architectures (**S3**, Figure 3c); b, prisms (3.8 mL HNO_3, Figure 6d); c, nanorods (0 g citric acid, Figure 7a). (The three samples are measured by using the same experimental conditions.)

The addition of citric acid also plays an important part in the formation of the final hierarchical architecture. It is known that citric acid possesses three carboxylic acid groups and one hydroxyl functional group, which can provide chelating ability and selectively bind to specific crystallographic facets. In the beginning of the reaction, citric acid reacts with the Ce^{3+} ions to form citrate complexes and decreases the concentration of the Ce^{3+} ions in the solution. After the addition of the phosphorus source, an ion-exchange reaction between PO_4^{3-} and citrate ions takes place, leading to the formation of $CePO_4$ under hydrothermal conditions. Reaction velocity can be adjusted through the slow release of the complex. At the same time, the special molecular structure of citric acid makes them selectively bind sideways to the pre-existing prisms,[33,34] which further induces the aggregation of the newly formed nuclei on the preformed prisms and forms the final flower-like hierarchical structures.

It should be noted that the addition of the ethanol also has an effect on the final morphology of the product by adjusting the viscidity and saturated vapor pressure of the solution under thermal conditions, which further effect the homogenization of the reactants in the reaction medium, the amount of the individual nuclei formed, and the amalgamation as well as the direction preference of growing nuclei[35] As described above, when the content of the ethanol increases, the viscidity of the solution decreases dramatically, which can create more chances for the Ce^{3+} ions and PO_4^{3-} ions to collide with each other and form nuclei. Under the cooperation of CTAB and citric acid, the following crystal splitting process is accelerated, which further induces the formation of the final 3D hierarchical architecture.

Figure 11 shows the excitation and emission spectra of the $CePO_4$ hierarchical architectures obtained at different reaction times. The excitation spectra show a broad band, which corresponds to the transitions from the ground $^2F_{5/2}$ to excited 5d states of the Ce^{3+} ions. The emission spectra exhibit a strong ultraviolet broad band centered at 344 nm, due to the 5d → 4f transition of the Ce^{3+} ions. From the emission spectra, it can be found that the intensity of the luminescence increases with a prolonging of the reaction time. In general, radiative mechanisms compete with nonradiative mechanisms, and the defects in materials can form quenching centers which lead to nonradiative recombination and luminescence quenching. Therefore, the difference in emission intensity should be mainly associated with the defects which come from the surface states of the prisms since the surface defects are a most important pathway for nonradiative relaxation in nanomaterials.[36] This result reveals that the crystal structure is perfected and the defects on the surface decrease gradually with increases in the reaction time.

Furthermore, the effect of the morphology on the luminescent properties of the products also has been investigated. Figure 12 shows the excitation and emission spectra of the $CePO_4$ with different morphologies. From the emission spectra, one can find that the intensity of the Ce^{3+} emission depends on the shape of the products. The intensity of flower-like hierarchical architectures (**S3**) is the weakest one, while that of the prisms obtained with 3.8 mL of HNO_3 added into the reaction solution is the strongest one of the three samples. One reason for the change in luminescent intensity is that the remnants of the organic reagents of CTAB and citric acid absorbed on products have a quenching effect on the luminescence of the products. Another reason for the variation is that the different surface defects of the products, which come from the surface states of the components, affect luminescent efficiency, because the defects in materials can lead to luminescence quenching. In addition, the complication of the morphology of the flower-like hierarchical architectures reduces the luminescence efficiency by reflecting part of the luminescence in the inner part of the architectures, which leads to the absorption of the defects in the flower-like hierarchical architectures. Therefore, the difference in the luminescent intensity of the products may be due to the remnants of the organic reagents of CTAB and citric acid absorbed on the samples, the defects on the surface, and the change of the morphology. The detailed mechanism behind morphology's influence on the properties of photoluminescence still needs further research.

4. Conclusion

In summary, spherical flower-like $CePO_4$ hierarchical architectures composed of numerous hexagonal prisms

(33) Kilin, D. S.; Prezhdo, O. V.; Xia, Y. N. *Chem. Phys. Lett.* **2008**, *58*, 113.
(34) Garcia, S. P.; Semancik, S. *Chem. Mater.* **2007**, *19*, 4016.
(35) Zhang, J.; Sun, L. D.; Yin, J. L.; Su, H. L.; Liao, C. S.; Yan, C. H. *Chem. Mater.* **2002**, *14*, 4172.
(36) Abrams, L.; Holloway, P. H. *Chem. Rev.* **2004**, *104*, 5783.

originating from the same center have been successfully obtained via a hydrothermal method. The investigation of synthesis parameters reveals that the coexistence of citric acid and CTAB in the reaction system should be responsible for the formation of the spherical flower-like $CePO_4$ hierarchical architectures. It is suggested that the growth process follows the crystal splitting theory. The luminescent properties exhibit that the intensity of the luminescence increases with the reaction time, revealing a decrease of the surface defects in the $CePO_4$ hierarchical architectures. It is also observed that the intensity of the Ce^{3+} emission depends on the shape of the products. These unique hierarchical architectures may have potential applications in the fields of optoelectronic devices. Moreover, our study may open a novel and facile route for the design and synthesis of inorganic functional materials with hierarchical architectures.

Acknowledgment. This work is financially supported by the National Natural Science Foundation of China (Grant No. 20771098) and the National Basic Research Program of China (973 Program, Grant Nos. 2007CB935502 and 2006CB601103).

Supporting Information Available: Figure showing the lower and higher magnifications of the product obtained without CTAB. This material is available free of charge via the Internet at http://pubs.acs.org.